Development of a high strength Al-Zn-Si-Mg-Cu alloy for selective laser melting

R. Casati[1,*], M. Coduri[2,3], M. Riccio[4], A. Rizzi[1,4], M. Vedani[1]

[1] Department of Mechanical Engineering, Politecnico di Milano, Via G. La Masa 1, 20156, Milano, Italy.

[2] ESRF, European Syncrotron Radiation Facility, Grenoble, France.

[3] Department of chemistry, University of Pavia, via Taramelli 12, 27100, Pavia, Italy

[4] Beam-IT, Strada Prinzera, 17, 43045, Fornovo di Taro (PR), Italy.

[*] riccardo.casati@polimi.it

Abstract

Despite additive manufacturing processes are already widely used in several industrial applications, there are few materials that are specifically designed and optimized for these technologies. Currently, only few Al alloys are available on the market and employed for 3D printing of structural parts. In particular, Si-Mg bearing alloys are the most common Al alloys for additive manufacturing, featuring high processability but moderate mechanical properties. By this work, we studied the effect of Si addition on the hot cracking susceptibility of a high strength Al-Zn-Mg-Cu alloy. A preliminary activity has been carried out by blending Al-Zn-Mg-Cu and Al-Si-Mg powders and analysing their microstructure and properties achieved after selective laser melting. Eventually a new Al-Zn-Si-Mg-Cu alloy has been designed, produced as powder alloy by gas atomization and tested. The microstructure and phase transformations of the new alloy has been investigated by synchrotron X-ray diffraction, differential scanning calorimetry and microscope analysis. The Al-Zn-Si-Mg-Cu alloy processed by selective laser melting featured a relative density of 99.8 %, no hot cracks were noticed within the investigated microstructures. The ability of the new alloy to respond to aging starting from both as built and solution annealed conditions has been also evaluated. A good response to direct aging (directly from as built condition) was demonstrated, featuring yield strength and ultimate tensile strength of 402 and 449 MPa, respectively, and hardness of 174 HV after optimized aging at 165°C for 2 hours.

Keywords

Metal Additive Manufacturing; High strength Al alloy; Synchrotron X-ray diffraction; Differential Scanning Calorimetry; Mechanical properties.

Introduction

Additive Manufacturing (AM) technologies allow building net-shape complex objects through a layer-by-layer addition of material. Among the AM technologies, Selective Laser Melting (SLM) is the most widespread powder-bed process. SLM employs a high-power laser beam to locally melt the material and allows producing parts with extremely complex shape [1].

Solidification in materials processed by SLM occurs very rapidly, out of equilibrium, leading to extended solid solutions and fine microstructures [2]. Generation of defect-free parts involves partial remelting of the previously solidified material that in turn is responsible for epitaxial grain growth and generation of crystallographic textures in the direction of heat extraction. Even though the primary phase quickly solidifies in supersaturated condition, the liquid near the solid interface enriches in solute, thus producing an undercooled condition. This is especially true if highly alloyed materials are considered. As a consequence, cellular growth of the solid phase is stimulated with liquid trapped in the channels between solidified regions. During the terminal stage of liquid-solid phase transformation, the solidification shrinkage and thermal contraction produce voids and hot tearing cracks in these channels, which may propagate through the full length of the columnar grains or even through adjacent intergranular regions in the most critical alloys [3-5]. Therefore, despite the high interest of industry in AM and the relatively high number of parts currently employed in many applications, only a limited number of alloys are available on the market. Indeed, many materials are susceptible to solidification cracking and can hardly be processed by 3D printing technologies [4,6]. As a general rule, most of the alloys that have poor weldability are normally barely processable by SLM [3,7].

Al alloys currently used for AM processes mostly derive from conventional cast alloy formulations, mainly Al-Si and Al-Si-Mg systems, featuring moderate strength and ductility [3]. Some studies have been carried out to tailor heat treatments of Al-Si-Mg alloys produced by SLM to improve their final strength [8-10]. Although positive results were achieved in these studies, the increase in strength that can be reached by these alloys is limited and they cannot attain the outstanding performance typically encountered in high-strength wrought alloys belonging to the 2xxx and 7xxx series.

A few attempts were made to improve processability of Cu-bearing Al alloys [6,11,12]. Van Humbeeck and co-workers investigated the effect of the addition of pure Si powder on the processability of the high strength 7075 Al alloy [11]. Silicon favoured the formation of crack-free microstructures, yet no information on tensile behaviour of the modified alloys was reported. In a further study, the same alloy was processed by introducing nanoparticles of nucleants to control solidification during additive manufacturing [12]. The fine equiaxed grain structure, which is promoted by the heterogeneous nucleation of grains, was able to better accommodate strain and to prevent cracking. A similar approach was used by Zhang et al. [6] to modify an Al-Cu-Mg alloy, but instead of using ex-situ nanoparticles, the authors modified the alloy composition with Zr, thus promoting the precipitation of Al_3Zr fine nucleants in the liquid melt.

By this work, the effect of Si addition on solidification behaviour of Al-Zn-Mg-Cu alloys processed by SLM was further investigated. Preliminary SLM prints and aging tests were performed by using two blends of gas atomized powders with similar particle size distribution. Namely, Al-9.7Si-0.5Mg and Al-8.2Zn-2.3Mg-1.6Cu (7068 alloy grade) powders were blended to produce two batches with a nominal Si content of 3 wt.% and 4.5 wt.% on average. Based on the microstructure and hardness results achieved, a new Al-8.2Zn-2.3Mg-1.6Cu alloy was designed, produced as powder alloy by gas atomization and processed by SLM. The solidification and aging behaviour of the alloy was studied by means of differential scanning calorimetry (DSC). Aging treatment was optimized based on peak-hardness criterion, by treating samples for different times at three temperature

levels, namely 135°C, 150°C and 165°C. The microstructures were characterized by electron and optical microscopy and by X-ray diffraction (XRD) by means of high-energy synchrotron radiation. Tensile properties of the alloy were assessed in the as built and aged conditions.

Experimental methods

Gas-atomized Al-Si-Mg (D_{10} = 6.7 µm, D_{50} = 22.5 µm, D_{90} = 43.5 µm, produced by EOS) and Al-Zn-Mg-Cu (D_{10} = 6.9 µm, D_{50} = 19.6 µm, D_{90} = 42.8 µm, produced by Kimera International-ECKA Granules) alloy powders were used for the experiments. The chemical composition of the as received materials and of the designed alloys used in present investigations is reported in Table 1. The Al-9.7Si-0.5Mg and Al-8.2Zn-2.3Mg-1.6Cu (7068 grade) powders were blended to obtain two batches containing on average 3 wt.% and 4.5 wt.% of Si, which were respectively named Alloy A and Alloy B. After optimization a new Al-Zn-Si-Mg-Cu alloy (D_{10} = 6.6 µm, D_{50} = 20.0 µm, D_{90} = 43.1 µm, produced by Kimera International-ECKA Granules) was proposed with the chemical composition also reported in Table 1 and labelled as Alloy C. The histogram in Figure 1 summarizes the amount of the main alloy elements in the investigated powders.

Table 1 Chemical composition (weight fraction, %) of the Al alloy powders used for the investigation.

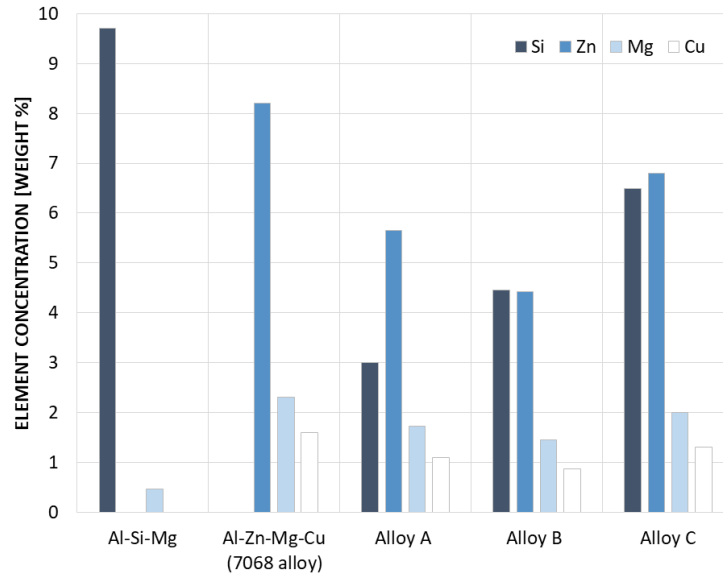|	Al-Si-Mg	Al-Zn-Mg-Cu (7068 alloy)	Alloy A (blend)	Alloy B (blend)	Alloy C Al-Zn-Si-Mg-Cu
Si	9.7	-	3.0	4.5	6.5
Zn	-	8.2	5.7	4.4	6.8
Mg	0.47	2.3	1.7	1.5	2
Cu	-	1.6	1.1	0.9	1.3
Fe	0.23	-	0.07	0.11	-
Zr	-	0.12	0.08	0.06	0.2
Ti	0.01	-	<0.01	<0.01	-
Mn	0.01	-	<0.01	<0.01	-
Al	bal.	bal.	bal.	bal.	bal.

Figure 1 Amount of the main alloying elements in the Al-Si-Mg, Al-Zn-Mg-Cu and Al-Zn-Si-Mg-Cu and blended powders, namely Alloy A with 3 wt.% of Si and Alloy B with 4.5 wt.% of Si.

A model 280 HL system by SLM Solutions GmbH was employed to produce cubic samples with side of 10 mm that were used for microstructural analysis and hardness tests and cylinders having a length of 80 mm and a diameter of 11 mm that were machined in form of dog-bone specimens for tensile tests. The 280 HL SLM Solutions system is equipped with a 280 x 280 x 365 mm^3 build chamber and twin optics. The process was carried out in an inert gas atmosphere of Argon.

Optimization of process parameters for each pre-alloyed and blended powder was carried out by a statistical design of experiment (DOE) approach using Minitab software. The choice of the optimal set of parameters was made based on the achieved material densities. A Central Composite Design (CCD) experimental plan has been designed by setting a minimum and a maximum value for two variables, namely power and laser speed. Hence, a set of 13 combinations of parameters were generated and assigned to the cubic samples of each build, including the central point that was replicated 5 times.

Table 2 shows the optimized parameters for the Alloy B and Alloy C. Optimal parameters for the processing of the 7068 alloy and for the Alloy A (3 wt.% Si) powders could not be defined, even though 8 builds were completed using volume energy densities spanning from 14 J/mm^3 to 100 J/mm^3. Indeed, extensive cracks formed within the microstructures, as it will be later shown in the section *Results*.

Table 2 Optimized SLM parameters used to process the Alloy B (4.5 wt.% Si) and the novel alloy C

	Alloy B	Alloy C
Platform Temperature (°C)	60	60
Hatch Distance (mm)	0.16	0.16
Laser Power (W)	350	200
Laser speed (mm/s)	1074	570
Layer Thickness (mm)	0.05	0.03
Scanning strategy	Stripes	Stripes

Solution annealing was performed for 1 h at 475°C, followed by water quenching. The temperature level was selected on the basis of solution annealing treatment of the parent alloy. Aging response of the SLM processed samples was evaluated starting from the as built and from the solution treated conditions. Isothermal aging tests were performed at 135°C, 150°C and 165°C for times ranging from 1 h to 64 h. The evolution of hardness after different aging times was tracked by Vickers indentations with a load of 300 g.

Microstructure analyses were carried out by optical microscope and scanning electron microscope (SEM) mod. Zeiss EVO 50 equipped with energy dispersive X-ray analysis, secondary electrons and back-scattered electrons (BSE) detectors. Samples were prepared by a standard grinding and polishing procedure. Chemical and electrolytic etchings were performed to reveal different microstructural features using Keller's and Barker's reagents, respectively.

Differential scanning calorimetry (DSC) analysis was carried out by a Setaram Labsys instrument in Ar atmosphere setting heating and cooling ramps at 10 °C/min with samples having a weight in the range 40-60 mg in the as built and solution treated starting conditions.

XRD investigation was performed at the ID22 beamline (High Resolution Powder Diffraction) of the European Synchrotron Radiation Facility (ESRF) in Grenoble (France), using the high resolution setup equipped with scintillator detectors, which employs crystal analysers to guarantee high resolution and suppress parasitic scattering [13]. Cylindrical specimens with 1 mm diameter were cut for facilitating rotation during acquisition, thus reducing preferred orientations, but still keeping absorption negligible. The incident monochromatic wavelength (λ = 0.4275 Å, 29 keV) was calibrated against a Si NIST standard. Data were processed with QualX software [14] for phase identification and with GSAS software [15] to estimate relative phase fractions and extract lattice parameters.

Tensile tests were performed at room temperature with a crosshead speed of 1.3 mm/min using a Zwick-Roell Z100 universal testing machine equipped with extensometer. The tensile specimens machined starting from the printed cylinders featured a gauge length of 30 mm and a gauge diameter of 6 mm. Tensile tests were performed on specimens printed with longitudinal axis both parallel (specimens labelled as V) and perpendicular (H) to the building direction. Four specimens were tested for each condition.

Results

a) SLM experiments on 7068 alloy, Alloy A and Alloy B

SLM builds were produced using the Al-8.2Zn-2.3Mg-1.6Cu (7068 grade) powder and blends of the Al-8.2Zn-2.3Mg-1.6Cu and Al-9.7Si-0.5Mg powder alloys, with the purpose of investigating the effect of Si on the processability of Al-Zn-Mg-Cu alloys. In particular, two blends were tested, namely Alloy A and Alloy B with a total amount of Si of 3 wt.% and 4.5 wt.%, respectively.

In Fig. 2, representative micrographs of the alloys processed by SLM are shown. As expected, although numerous 7068 alloy samples were printed by setting a wide range of energy densities, spanning from 14 J/mm^3 to 100 J/mm^3, crack-free microstructures could not be achieved. A representative micrograph of the section perpendicular to the building direction of a 7068 alloy sample is reported in Fig. 2a. The micrograph shows that cracks extend throughout the microstructure according to an almost regular pattern. The micrograph of a section taken parallel to the building direction reported in Fig. 2b shows that the main cracks propagate along the columnar grain boundaries parallel to the building direction. Solidification cells surrounded by discrete particles are noticeable at higher magnification, as depicted by the SEM-BSE image of Fig. 2c. The second phases are indicated with arrow in the figure. The samples of Alloy A (3 wt.% Si) exhibit less cracks, as depicted in Fig. 2d, whereas those of Alloy B (4.5 wt.% Si) showed no cracks, even in high magnification images. Full density was achieved in these latter samples, as revealed by micrographs in Fig. 2e and Fig 2f. The SEM image in Fig. 2f shows a microstructure made up of solidification cells smaller than those of the 7068 alloy (compare with figure Fig. 2c) and decorated at boundaries by abundant solute segregations. This is consistent with theories regarding formation of solidification cells in Al alloys produced by SLM [16].

Fig. 3 shows the microstructure of the Alloy B after the solution annealing treatment performed for 1 h at 475°C followed by water quenching. Solidification cells are no longer visible and second-phase particles, with a size smaller than 2 μm, homogeneously distributed within the aluminium matrix appeared.
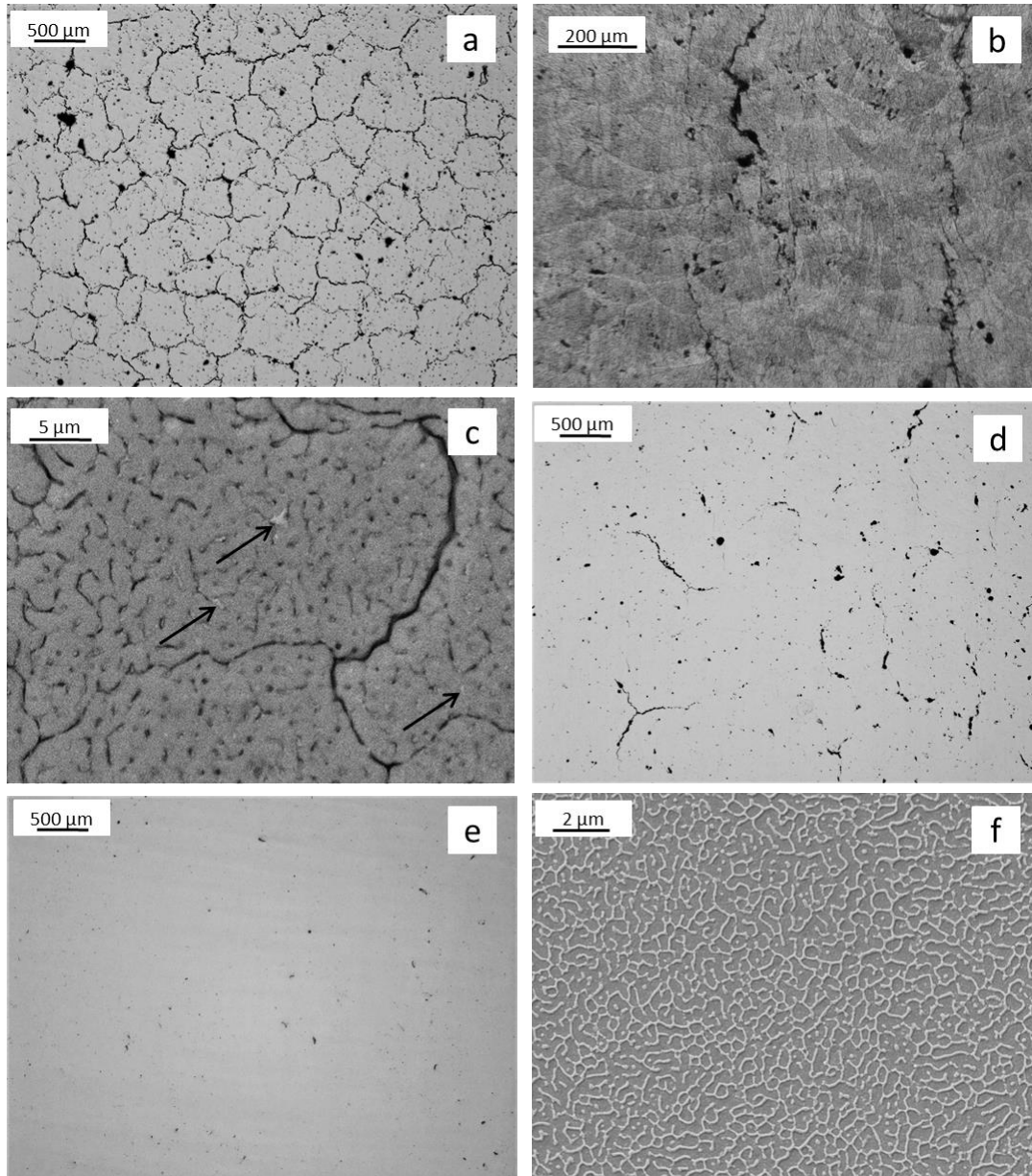
Figure 2 Optical micrographs of the section a) perpendicular and b) parallel to the building direction of the as built 7068 alloy; c) high magnification SEM image of the as built 7068 alloy; d) optical micrographs of the as built Alloy A containing 3 wt.% Si e) and Alloy B containing 4.5 wt.% Si (sections perpendicular to the building direction); f) high magnification SEM image of the as built Alloy B.
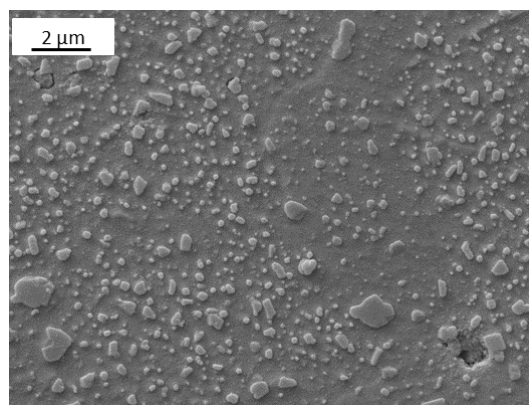
Figure 3 SEM image of the Alloy B (4.5 wt.% Si) after solution treatment performed at 475°C for 1 h followed by water quenching.

Aging curves for the Alloy B were collected by performing heat treatments at different temperatures and for different times, starting from as built and from solution annealed samples. The results are reported in the diagram of Fig. 4. The graph shows that solution treatment was responsible for a drastic decrease in hardness. Indeed, as built samples feature a micro-hardness of 112 HV, which drops down to 77 HV after solubilisation. The hardness of the as built alloy increases up to 153 HV when the material is treated for 24 h at 135°C. If the alloy is aged at 150 °C or 165 °C, maximum achievable hardness is slightly lower but, as expected, it is reached in shorter times. Isothermal aging performed at 135°C is also responsible for an increase in hardness of the solution annealed alloy. The specimens treated for 24 h at 135°C reached a maximum hardness of 112 HV.
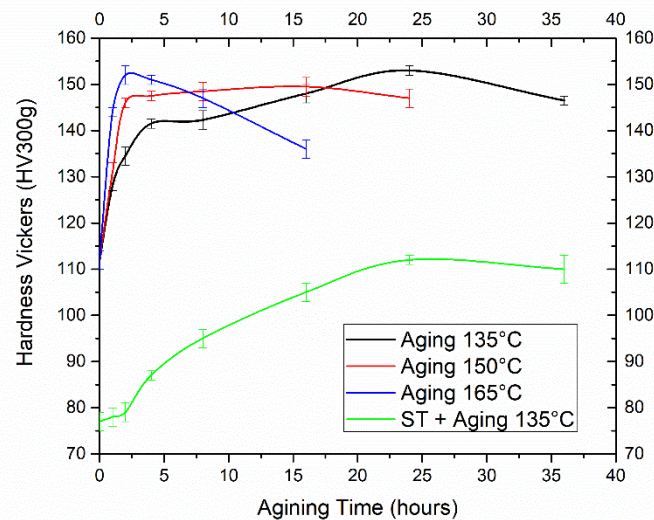

Figure 4 Aging curves (HV vs. aging time) of Alloy B collected at different temperatures (135°C, 150°C and 165°C) starting from the as built and from solution annealed conditions.

Based on the results achieved using the powder blends of Al-Zn-Mg-Cu and Al-Si-Mg powders, a new Al-Zn-Si-Mg-Cu alloy (named as Alloy C) was designed, atomized as pre-alloyed powder and SLM tested. As compared to the composition of Alloy A and Alloy B, the chemical composition of the new alloy features higher amount of precipitate-forming elements (Zn = 6.8 wt.%, Cu = 2.0 wt.%, Mg = 1.3 wt.%) that are expected to further improve hardness and strength of the material. An higher amount of Si (6.5 wt.%) was also considered to ensure SLM processability even for more critical sample geometries (see Table 1).

b) SLM experiments on Alloy C powders

The gas atomized Alloy C (Al-6.8Zn-6.5Si-2Mg-1.3Cu) that was specifically produced based on the designed composition revealed good processability by SLM. Relative density of 99.8 % was achieved in printed samples and no cracks were found within the investigated microstructures, as depicted by the representative optical micrograph given in Fig. 5a. After chemical etching, solidified melt pools were visible (Fig. 5b). At higher magnification (Fig. 5c), the SEM image shows that grains are made up of solidification cells with solute-rich regions surrounding their boundaries. The microstructure of the novel Alloy C was similar to that displayed by the Alloy B (compare with Fig. 2f).

The solidification behaviour of the Alloy C (Al-6.8Zn-6.5Si-2Mg-1.3Cu), Al-9.7Si-0.5Mg and Al-8.2Zn-2.3Mg-1.6Cu (7068) alloys was compared by means of DSC analyses, as reported in Fig. 6a. The cooling curve of the Al-8.2Zn-2.3Mg-1.6Cu alloy shows one large exothermic peak spanning from 635°C to 550°C. A second small exothermic peak appears at lower temperatures, as indicated by the arrow in the magnified section of the same graph reported in the inset. The curve of the Al-9.7Si-0.5Mg alloy exhibits two sharp exothermic peaks. Based on well established solidification behaviour of Al-Si-Mg casting alloys, the peak occurring at the highest temperature is attributed to the formation of the primary α-Al phase, the second peak is related to the formation of the binary eutectic constituent [17]. Finally, the solidification curve of the Alloy C displays two main peaks as well. In particular, it is believed that the one arising at the highest temperature is due to the formation of the primary α-Al phase, whereas the one at lower temperature is produced by the superposition of heat contributions given by multiple exothermic reactions.

The XRD pattern collected on Alloy C specimens is displayed in Fig. 7a. The goal of XRD analysis was to investigate the nature of second phases formed during alloy solidification and cooling exploiting the high signal-to-noise ratio provided by synchrotron data. The scattering is dominated by the FCC signals of Al, peaks of second phases have much lower intensity, as shown in Fig. 7b and Fig.7c. Indeed, the intensity of the strongest signal in the background is only 0.25% that of the (111) Al reflection (Fig. 7). Eventually, the high resolution setup allowed to resolve peaks with very similar d-space and to detect variations in peak shape, correlated to extended defects, as the instrumental contribution to peak broadening is negligible [13]. XRD measurements were performed using a rotating stage that helped mitigating preferred orientations effects, thus providing more reliable peak intensities. Rietveld refinements were used to estimate lattice parameters and phase fractions. Phases were considered as reliable when all major expected reflections were observed in the pattern and when intensities were in accordance to expected proportion.

The main secondary phase in the novel Alloy C is Si (estimated in a concentration of 2.8 wt.%). Compared to the other lines, Si peaks are much broader. This is consistent with a crystallite size limited to about 10 nm, as estimated by Scherrer formula [18] applied to the first (111) Si reflection. Crystallite size is consistent with previous investigation on Al-Si-Mg system produced by SLM [2]. As displayed in Fig. 7b, many other low-intensity reflections were observed. Besides Si, very small amount (< 0.1%) of Cu (*Fm*-3*m*, a=3.63 Å) and Zn (*P*6$_3$/*mmc*, a=2.675 Å, c=4.945 Å) were also observed (see dashed lines in Fig. 7b).

The XRD interpretation of possible intermetallics is reported in Fig. 7c. The presence of low angle peaks indicates a bigger unit cell than for the above single metals. Indeed, the first peak corresponds to an interplanar distance of 8.93 Å. Li and Starink [19] summed up the main precipitates in Al-rich system containing Zn, Cu and Mg, together with the different notations

according to composition. Our data support the presence of a small amount of θ phase, Al_2Cu (0.2 %, *I4/mcm*, *a*=6.062 Å, *c*=4.872 Å) [20], since all its major reflections are observed. This is not the case for $MgZn_2$ (phase μ, isostructural to AlCuMg), the presence of which is doubtful as some of the expected reflections were not observed. The same applies to the secondary phases Z (Mg_2Zn_{11}, $Cu_6Mg_2Al_5$), S (Al_2CuMg) and T (AlMgZn, $CuMg_4Al_6$).

Some of the reflections are consistent with quaternary Q-phase $Al_4Cu_2Mg_8Si_7$ [21,22] (1.7%, *P-6*, *a* = 10.30 Å, *c* = 3.97 Å), sometimes reported as $Al_{1.9}CuMg_{4.1}Si_{3.3}$ [23]. Another quaternary phase consistently detected by our XRD data is $Al_8Si_6Mg_3Fe$ [24] (0.6 %, *P-62m*, *a* = 6.63 Å, *c* = 7.95 Å), with Fe being considered as a known impurity. Still, some peaks remain unassigned. We can speculate that they might be related to some complex intermetallics. The ternary compound $Si_7Mg_6Cu_{16}$ (*a* = 11.65 Å) [25] is consistent with many experimental peaks, but not all expected reflections are observed. This could indicate some preferred orientations or a different structure with respect to those reported in the literature. Similarly, we cannot exclude the presence of $FeSiAl_5$ (*A2/a*, *a* = 6.167 Å, *c* = 20.809 Å, the reported structure is for $FeSiAl_{4.5}$ in [26]). Otherwise, some signals can be related to different compositions of phases already considered. As an example, a satellite signal occurs on the right of the Q-phase peaks, with the splitting increasing with the scattering angle. This could be consistent with a smaller unit cell, containing excess of small atoms such as Si or Cu, or other impurities.
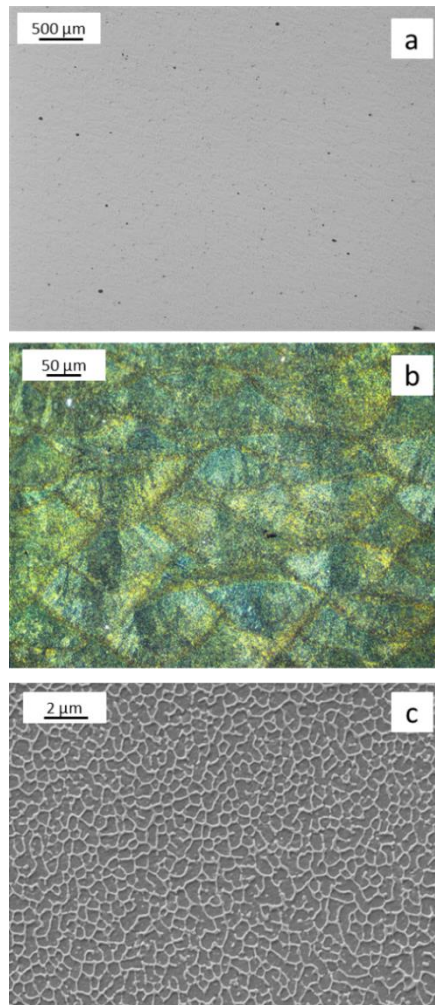
Fig. 5 Micrographs of the section parallel to the building direction of the as built Alloy C (Al-6.8Zn-6.5Si-2Mg-1.3Cu): low magnification optical micrographs of the a) unetched and b) etched material and c) SEM image of the alloy after etching.
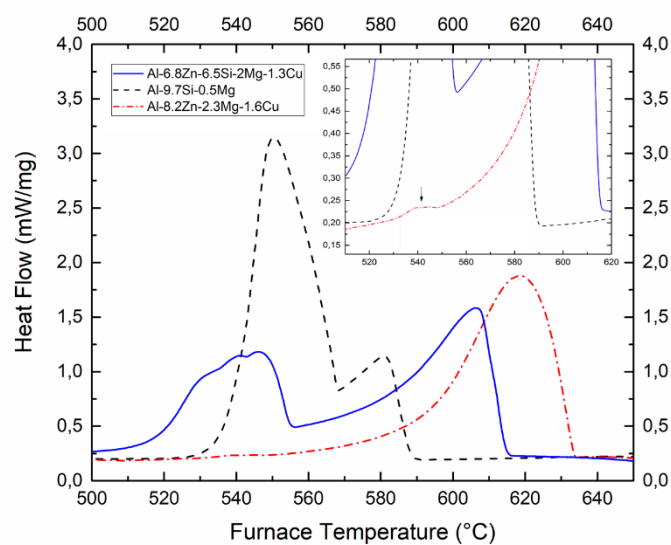

Figure 6 DSC cooling curves of the Al-6.8Zn-6.5Si-2Mg-1.3Cu, Al-9.7Si-0.5Mg and Al-8.2Zn-2.3Mg-1.6Cu. A magnified portion of the graph is reported in the inset.
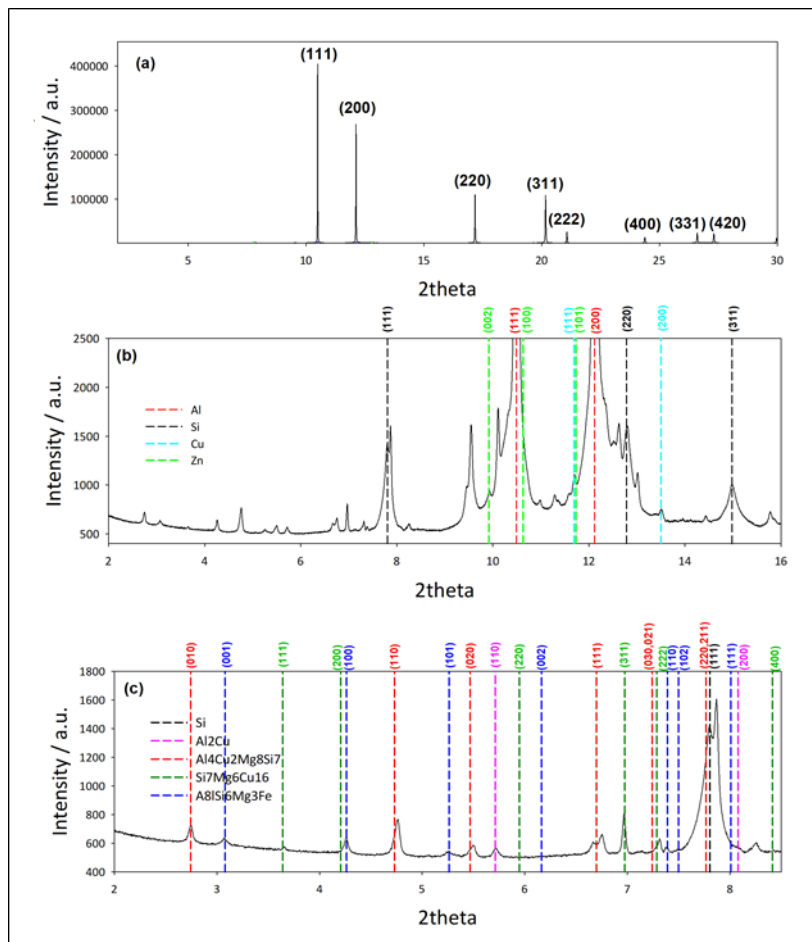
Figure 7. XRD phase identification: a) full pattern showing Al peaks; b) single element phases; c) intermetallics at low angle.

DSC analysis was performed also on the Alloy C processed by SLM to investigate its aging behaviour. A representative heating ramp of the as built alloy is reported in Fig. 8. A wide exothermic peak, labelled as A, is detected between 180°C and 290°C and it is followed by a second exothermic peak, named as B. The magnified view of the curve in the region of peak A shown in the inset suggests that this peak is generated by the superposition of several exothermic effects, highlighted by arrows. The exothermic peaks can be attributed to the precipitation of different species, as discussed later. Thus, the as built condition can be considered as a suitable condition for an effective dispersion strengthening process by artificial aging treatment.
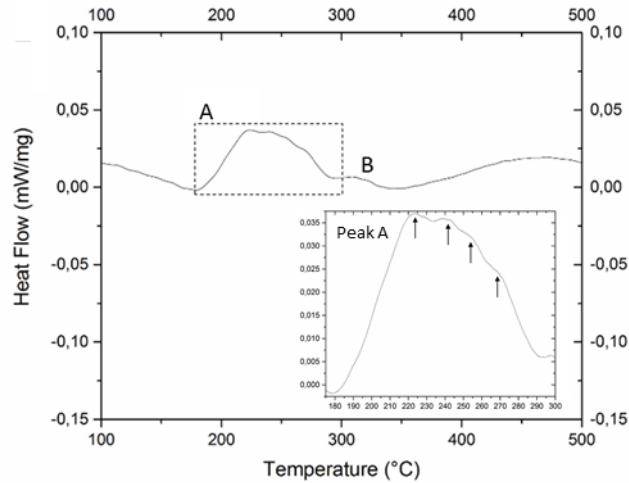
Figure 8 DSC heating curve (heating rate 10°C/min) of Alloy C (Al-6.8Zn-6.5Si-2Mg-1.3Cu). A magnified portion of the graph is reported in the inset.

Isothermal aging tests were conducted at 135°C, 150°C and 165°C on as built Al-6.8Zn-6.5Si-2Mg-1.3Cu alloy. The aging curves (hardness vs. aging time) are depicted in Fig. 9. The general trends are similar to those already shown by the Alloy B and reported in Fig 4, but higher hardness values are achieved by the Alloy C. The as built sample exhibits a hardness of 141 HV that increases to a peak value of 174 HV after artificial aging for 4 h at 165°C. Thermal aging performed at 150°C for 16 h and at 135°C for 24 h leads to hardness values of 172 HV and 170 HV, respectively.
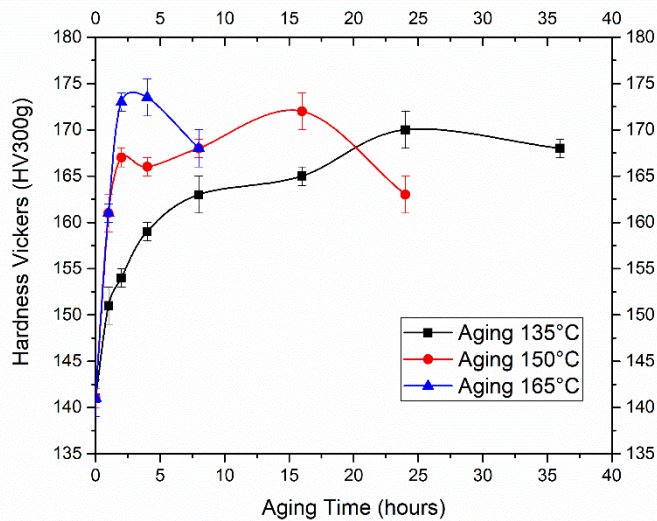

Figure 9 Aging curves (HV vs. aging time) of Alloy C collected at different temperatures (135°C, 150°C and 165°C) starting from the as built condition.

The tensile properties of the as built and peak-aged Alloy C are collected in Table 3. Representative stress-strain curves are also reported in Fig. 10. The as built H and V samples exhibit yield strength (YS) of 332 and 313 MPa, ultimate tensile strength (UTS) of 447 and 386 MPa, and elongation at fracture of 2.3 % and 2.2 %, respectively. The aging performed right after

the SLM process at 165°C for 2 h (without any preliminary solution annealing), increased YS and UTS of the H specimens up to 402 MPa and 449 MPa, respectively, and those of the V specimens up to 370 MPa and 432 MPa, respectively. The elongation at fracture reduced to about 1.3% for both orientations.

Table 3 Average yield strength (YS), ultimate tensile strength (UTS) and elongation at fracture (ε_r) of the Alloy C (Al-6.8Zn-6.5Si-2Mg-1.3) in the as built and aged (T5 temper) conditions. Standard deviations are reported in brackets.

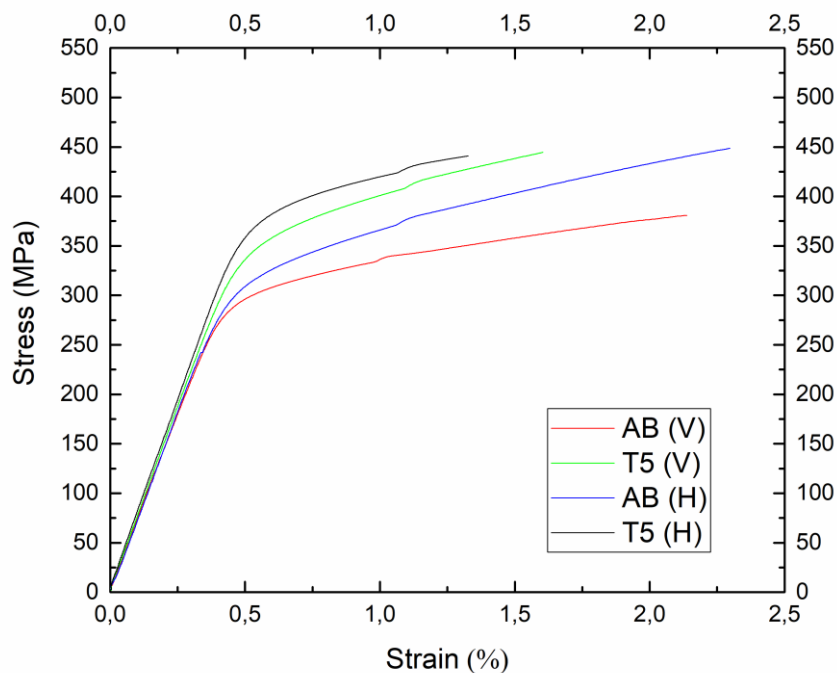|	YS [MPa]	UTS [MPa]	ε_r [%]
As built (V)	313 (8)	386 (16)	2.2 (0.4)
T5 temper (V)	370 (3)	432 (9)	1.4 (0.2)
As built (H)	332 (3)	447 (10)	2.3 (0.3)
T5 temper (H)	402 (4)	449 (12)	1.3 (0.2)

Fig. 10 Representative stress-strain curves.

Discussion

DSC analysis of the investigated alloys shows that the addition of Si promotes a marked modification of the solidification process of the Al-Zn-Mg-Cu alloy (Fig. 6). The unmodified alloy exhibits a big exothermic peak due to the formation of the primary α-Al phase. A low-enthalpy second peak occurs at lower temperatures and can be ascribed to solidification of minor second phases. The Al-Si-Mg alloy presents instead two peaks, the first occurring at higher temperatures

due to the analogous solidification of the α-Al phase, the second related to the formation of the binary Al-Si eutectic [17]. The Alloy C (Al-6.8Zn-6.5Si-2Mg-1.3Cu) exhibits two large exothermic peaks as well. As for the previous case, the former peak can be attributed to the solidification of the primary α-Al phase, whereas the latter to the formation of second phases and in particular to the formation of the binary Al-Si eutectic constituent and other phases, such as the quaternary Q-phase ($Al_4Cu_2Mg_8Si_7$) as shown by the XRD investigation.

Addition of silicon to the investigated Al-Zn-Mg-Cu alloys markedly reduced or hindered solidification cracks formed during SLM processing. As for welding and casting alloys, the temperature range at which a small fraction of liquid exists is considered as the most vulnerable interval, because the melt flow is restricted by narrow channels and solidification cracking is more likely to occur in the intergranular regions due to large shrinkage tensile stresses. The wider the vulnerable range of temperature, the higher the susceptibility to hot cracking. Indeed, a larger interval leads to extensive solidification shrinkage and thermal contraction, which translate into higher tensile stresses between adjacent grains [5,11]. Through the integration of the heat flow within the solidification temperature range, the trend of the solid fraction as a function of the temperature was plotted for the investigated Alloy C (Al-6.8Zn-6.5Si-2Mg-1.3Cu), Al-9.7Si-0.5Mg alloy and 7068 alloy (Al-8.2Zn-2.3Mg-1.6Cu) in the diagram of Fig. 11. These curves clearly show that Si does reduce the vulnerable interval of temperature. The presence of an abundant liquid in the last stage of solidification more easily feeds intergranular regions and heals incipient cracks. In good agreement with this observation, microscope investigations show that grains of the unmodified Al-Zn-Mg-Cu alloy are made up of primary Al cells with small and discrete second phases in their intercellular regions (Fig. 2c), whereas in the more processable Al-Zn-Si-Mg-Cu alloys, solidification cells are surrounded by a continuous and more abundant segregation network (Fig. 2f and Fig. 5c). The XRD analysis revealed that the Al-Zn-Si-Mg-Cu alloy has a richer microstructure consisting of several phases that compose the intercellular network. Besides the large concentration of Si and traces of Cu and Zn, significant amounts of θ (Al_2Cu) and Q (AlCuMgSi) phases were identified.

DSC scans also proved that the as built condition can be considered as suitable for being directly aged, thus skipping the solution treatment and water quenching steps. Indeed, the multiple exothermic peaks raised in the curve of the Al-Zn-Si-Mg-Cu alloy between 180°C and 330°C can be attributed to the formation of several precipitates. Previous works demonstrated that several stable-phases can precipitate in Al-Si-Cu-Mg alloys upon heating, namely β (Mg_2Si), θ (Al_2Cu) and Q ($Al_4Cu_2Mg_8Si_7$ [21] or $Al_5Cu_2Mg_8Si_6$ [27]) that are anticipated by the respective precursors (GP, β'', β', θ', Q'', and Q' metastable phases) [28-30]. In ref [31], it was shown that S' (Al_2CuMg) precipitates can also form in Al-Si-Cu-Mg alloys in T5 condition and in ref. [2] it was proved that Si can precipitate from supersaturated solid solution of Al-Si-Mg alloys processed by SLM. In addition, in Zn-Mg bearing Al alloys, η' (metastable) and η (stable $MgZn_2$) precipitates can sequentially form during thermal aging. This intricate scenario makes a confident and more precise identification of all the phases based on the onset and peak temperatures determined by DSC curves uncertain. Thus, it can be speculated that several phases form on heating, likely following the Al-Si-Cu-Mg and the Al-Zn-Mg alloy precipitation sequences. Dedicated and more detailed microscope analyses are needed for a more reliable and complete determination of the strengthening phases.
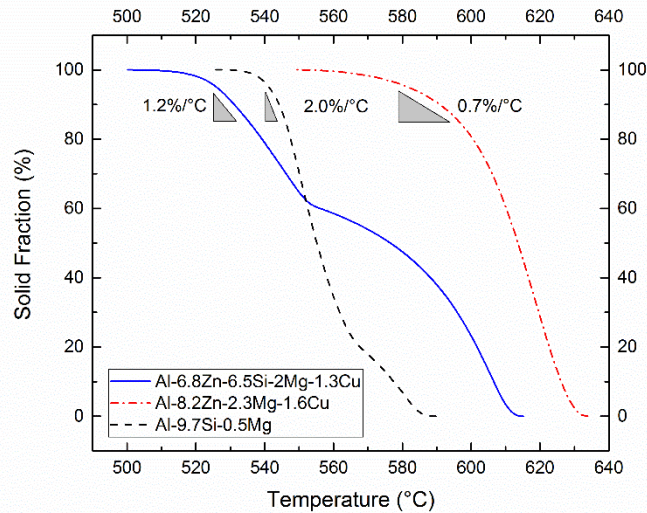
Fig. 11 Solidification curves for the investigated Al alloys, namely Al-6.8Zn-6.5Si-2Mg-1.3Cu, Al-9.7Si-0.5Mg and Al-8.2Zn-2.3Mg-1.6Cu.

The hardness vs. time curves reported in Fig. 4 and Fig. 9 clearly demonstrate that the standard thermal treatment procedures (solution treatment, water quenching and isothermal aging, i.e. T6 temper) might be deleterious when trying to improve material hardness after SLM processing. Solution treatment followed by water quenching led to a drop in hardness of the Al-Zn-Si-Mg-Cu alloy with 4.5 wt.% of Si from 112 HV to 77 HV. Following aging, enhanced material hardness is reached but the maximum achieved value of 112 HV does not exceed the value of the untreated as built material. It has been shown in several studies that a valid alternative strategy for several Fe- and Al-based alloys consists in promoting precipitation strengthening right from the rapidly solidified as built material [2,8,32-34]. The present finding confirms that the precipitation reaction can be effectively exploited starting from the supersaturated solution already formed upon cooling from SLM processing temperature also in the investigated Al-Zn-Si-Mg-Cu alloys and it can lead to an appreciable increase in hardness and mechanical strength. This kind of T5 temper increased the yield strength by 70 MPa and 57 MPa in the horizontal (H) and vertical direction (V), respectively (see Table 3 and Fig. 9). As expected, the Alloy C achieved a higher peak hardness (174 HV) than that showed by the Alloy B (153 HV). The gap can be reasonably ascribed to the higher amount of precipitate-forming elements contained in the pre-alloyed gas atomized powder. The yield strength values achieved by the proposed Al-6.8Zn-6.5Si-2Mg-1.3Cu alloy in T5 temper are about 90 MPa and 80 MPa higher than those exhibited by the AlSi7Mg-T5 and AlSi10Mg-T5 alloys produced by SLM, both considering the horizontal and vertical directions. Contrarily, lower levels of elongation at fracture are attained by the investigated alloy [2,8]. Considering high performance Al cast grades [35], yield and tensile strengths of the Al-6.8Zn-6.5Si-2Mg-1.3Cu alloy are comparable or even higher than those of the age hardenable Al-Cu alloys (i.e. 201-T6, 206-T6, 222-T62), whereas ductility is slightly lower. Indeed, high strength 2xx cast Al alloys are characterized by elongation at fracture typically higher than 4%. Further development may consider a slight reduction in strengthening element content or different thermal treatments, so as to increase material ductility with a limited loss in strength.

Conclusions

Based on the experimental results achieved, the following conclusions can be drawn:

- Silicon addition has a positive effect on the SLM processability of the investigated high-strength Al-Zn-Si-Mg-Cu alloys. The formation of eutectic constituents in the final stages of solidification reduces the vulnerable range of solidification and improves liquid feeding in the intergranular regions.
- XRD analyses confirmed the presence of Si (2.8 wt.%), $Al_4Cu_2Mg_8Si_7$ (1.7%), $Al_8Si_6Mg_3Fe$ (0.6 %), and small amount (< 0.1%) of Cu, Zn and Al_2Cu in the as built condition of the proposed Al-6.8Zn-6.5Si-2Mg-1.3Cu alloy.
- From isothermal aging curves, it can be inferred that solidification and cooling rates induced by SLM processing are fast enough to generate supersaturated solid solutions with full aging potential. Additional post-SLM solution annealing treatment is therefore not necessary as it promotes a significant depletion in the achievable strengthening.
- The proposed Al-6.8Zn-6.5Si-2Mg-1.3Cu alloy in T5 temper exhibited hardness of 174 HV, YS of 370 and 402 MPa and UTS of 432 and 449 MPa in the vertical and horizontal directions, respectively.

References

[1] D. Herzog, V. Seyda, E. Wycisk, C. Emmelmann, Additive manufacturing of metals, Acta Materialia 117 (2016) 371-392.

[2] R. Casati, M. Hamidi Nasab, M. Coduri, V. Tirelli and M. Vedani, Effects of Platform Pre-Heating and Thermal-Treatment Strategies on Properties of AlSi10Mg Alloy Processed by Selective Laser Melting, Metals 8 (2018) 954.

[3] T. DebRoy, H.L. Wei, J.S. Zuback, T.Mukherjee, J.W.Elmerb, J.O.Milewskic, A.M.Beesea, A.Wilson-Heida, A.Ded, W.Zhange, Additive manufacturing of metallic components – Process, structure and properties, Progress in Materials Science 92 (2018) 112.

[4] E. Chauvet, P. Kontis, E.A. Jägle, B. Gault, D. Raabe, C. Tassin, J.-J. Blandin, R. Dendievel, B. Vayre, S. Abed, G. Martin, Hot cracking mechanism affecting a non-weldable Ni-based superalloy produced by selective electron Beam Melting, Acta Materialia 142 (2018) 82-94.

[5] Sindo Kou, Welding Metallurgy Published by John Wiley & Sons, Inc., Hoboken, New Jersey.

[6] H. Zhang, H. Zhu, X. Nie, J. Yin, Z. Hu, X. Zeng Effect of Zirconium addition on crack, microstructure and mechanical behaviour of selective laser melted Al-Cu-Mg alloy, Scripta Materialia 134 (2017) 6-10.

[7] T. Mukherjee, J. S. Zuback, A. De & T. DebRoy Printability of alloys for additive manufacturing Scientific Reports 6 (2016) 19717.

[8] R. Casati, M. Vedani Aging response of an A357 Al alloy processed by Selective Laser Melting, Advanced Engineering Materials 1800406 (2018) 1-7.

[9] J. Fiocchi, A. Tuissi, P. Bassani, C.A. Biffi, Low temperature annealing dedicated to AlSI10Mg selective laser melting products, Journal of Alloys Compounds 696 (2017) 3402–3409.

[10] S. Marola, D. Manfredi, G. Fiore, M.G. Poletti, M. Lombardi, P. Fino, L.A. Battezzati, Comparison of Selective Laser Melting with bulk rapid solidification of AlSi10Mg alloy, Journal of Alloys and Compounds 742 (2018) 271–279.

[11] M.L. Montero Sistiaga, R. Mertens, B. Vrancken, X. Wang, B. Van Hooreweder, J.P. Kruth, J. Van Humbeeck, Changing the alloy composition of Al7075 for better processability by selective laser melting. Journal of Materials Processing Technology 238 (2016) 437–445.

[12] J.H. Martin, B.D. Yahata, J.M. Hundley, J.A. Mayer, T.A. Schaedler, T.M. Pollock, 3D printing of high-strength aluminium alloys, Nature 366 (2017) 365-369.

[13] J.-L. Hodeau, P. Bordet, M. Anne, A. Prat, A. N. Fitch, E. Dooryhee, G. Vaughan, A. K. Freund, Nine-crystal multianalyzer stage for high-resolution powder diffraction between 6 keV and 40 keV, Proceedings 3448, Crystal and Multilayer Optics, 1998.

[14] A. Altomare, N. Corriero, C. Cuocci, A. Falcicchio, A. Moliterni, R. Rizzi, QUALX2.0: a qualitative phase analysis software using the freely available database POW_COD. Journal of Applied Crystallography 48 (2015) 598-603.

[15] A.C. Larson, R.B. Von Dreele, General Structural Analysis System (GSAS), Los Alamos National Laboratory Report LAUR (2004) 86–748.

[16] Prashanth K GJ. Eckert, Formation of metastable cellular microstructures in selective laser melted alloys, Journal of Alloys and Compounds 707 (2017) 27-34

[17] Q.G. Wang, C.J. Davidson "Solidification of precipitation behaviour of Al-Si-Mg casting alloys. Journal of Materials Science 36 (2001) 739-750.

[18] P. Scherrer, Göttinger Nachrichten Gesell. 2 (1918) 98.

[19] X.-M. Li and M. J. Starink, The Effect of Compositional Variations on the Characteristics of Coarse Intermetallic Particles in Overaged 7xxx Al Alloys, Materials Science Technology, 17 (2001) 1324-1328.

[20] Y. Grin, F.R. Wagner, M. Ambruester, M. Kohout, A. Leithe Jasper, U. Schwarz, U. Wedig, H.G. von Schnering, CuAl2 revisited: Composition, crystal structure, chemical bonding, compressibility and Raman spectroscopy, Journal of Solid State Chemistry 179 (2016) 1707-1719.

[21] L. Arnberg, B. Aurivillius, The crystal structure of AlxCu2Mg12–xCu7, (h-AlCuMGSi), Acta. Chemica Scandinavica A 34 (1980) 1-5.

[22] A. K. Gupta, A. K. Jena & M. C. Chaturvedi, Insoluble phase in Al–1·52Cu–0·75Mg alloys containing silicon, Materials Science and Technology 12 (1987) 1012-1018.

[23] Vaumoussed Ceresoa, An atom probe study of tine scale structure in AlMgSi(Cu) alloys, Materials Science Forum 396402 (2002) 693-698.

[24] S. Foss, A. Olsen, C. J. Simensen, J. Tafto, Determination of the crystal structure of the pi-(Al Fe Mg Si) phase using symmetry- and site.sensitive electron microscope techniques. Acta Crystallographica B: structural science 59 (2003) 36-42.

[25] G. Bergman, L. H. Waugh, The crystal structure of the intermetallic compound Mg6Si7Cu16, Acta Crystallographica, 9 (1956) 214-217.

[26] V. Hansen, B. Hauback, M. Sundberg, C.Romming, J. Gjonnes, β-Al4.5FeSi: A Combined Synchrotron Powder Diffraction, Electron Diffraction, High-Resolution Electron Microscopy and Single-Crystal X-ray Diffraction Study of a Faulted Structure, Acta Christallographica 54 (1998) 351-357.

[27] L. Sagalowicz, G. Lapasset, G. Hug, Transmission electron microscopy study of a precipitate whichforms in the Al-Mg-Si system, Philosophical Magazine Letters 74 (1996) 57-66.

[28] Y.J. Li, S. Brusethaug, A. Olsen, Influence of Cu on the mechanical properties and precipitation behavior of AlSi7Mg0.5 alloy during aging treatment, Scripta Materialia 54 (2006) 99-103.

[29] E. Sjolander, S. Seifeddine The heat treatment of Al-Si-Cu-Mg casting alloys, Journal of material processing technology 210 (2010) 1249-1259.

[30] G. Wang, Q. Sun, L. Feng, L. Hui, C. Jing, Influence of Cu content on ageing behavior of AlSiMgCu cast alloys, Materials & Design 28 (2007) 1001-1005.

[31] R.K. Mishra, G.W. Smith, W.J. Baxter, A.K. Sachdev, V. Franetovic, The sequence of precipitation in 339 aluminum castings, Journal of Materials Science 36 (2001) 461-468.

[32] R. Casati, J. N. Lemke, A. Tuissi and M. Vedani, Aging Behaviour and Mechanical Performance of 18-Ni 300 Steel Processed by Selective Laser Melting, Metals 6 (2016) 218.

[33] R. Casati, J. N. Lemke, A. Zanatta Alarcón, M. Vedani Aging, Behavior of High-Strength Al Alloy 2618 Produced by Selective Laser Melting, Metallurgical and Materials Transactions A 48 (2016) 575-579.

[34] R. Casati, M. Coduri, N. Lecis, C. Andrianopoli, M. Vedani Microstructure and mechanical behavior of hot-work tool steels processed by Selective Laser Melting, Materials Characterization 137 (2018) 50-57.

[35] ASM handbook Volume 2. Properties and selections: non-ferrous alloys and special properties materials, ISBN: 978-0-87170-378-1.